Available online at www.sciencedirect.com
ScienceDirect
Ceramics International 37 (2011) 957–963
CERAMICS INTERNATIONAL
www.elsevier.com/locate/ceramint

Pulsed electric current sintering of transparent Cr-doped Al_2O_3

Khanh Quoc Dang [a], Shinichi Takei [b], Masakazu Kawahara [c], Makoto Nanko [a,*]

[a] Department of Mechanical Engineering, Nagaoka University of Technology, Kamitomiokamachi 1603-1, Nagaoka, Niigata 940-2188, Japan
[b] SINTERLAND Inc., 123 Amaike, Nagaoka, Niigata 940-2055, Japan
[c] SPS SYNTEX Inc., 3-2-1 Sakato, Takatsu, Kawasaki, Kanagawa 213-0012, Japan

Received 16 June 2010; received in revised form 2 October 2010; accepted 2 November 2010
Available online 2 December 2010

Abstract

Pulsed electric current sintering (PECS) was applied to obtain transparent ruby polycrystals. Al_2O_3–Cr_2O_3 powder mixture was prepared by drying an aqueous slurry consisting of Al_2O_3 and $Cr(NO_3)_3$ followed by PECS consolidation in vacuum at a sintering temperatures ranging from 1100 to 1300 °C with various heating rates between 2 and 100 °C/min and under an applied pressures from 40 to 100 MPa. Slow heating rate and high-pressure lead to highly densified and transparent Cr-doped Al_2O_3 polycrystals at sintering temperature of 1200 °C.

Keywords: B. grain size; Pulsed electric current sintering; Transparent; Cr-doped Al_2O_3

1. Introduction

The mineral corundum is a crystalline form of Al_2O_3. A pure crystal of corundum is the second hardest natural mineral on the earth known to mankind, transparent and perfectly colorless. Small amounts of metallic elements such as chromium, iron, titanium or vanadium can substitute for aluminum in the corundum crystal structure, giving rise to many color variations. Ruby, which is the red variety of corundum, consists of Cr-doped Al_2O_3 as well as very fine traces of other elements. With many favorable features such as high heat-resistance, high mechanical strength and excellent chemical stability, ruby is widely used in jewellery, mechanical parts like wear surfaces and precision balls and optics as solid-state lasers, lenses and prisms [1–4].

Pulsed electric current sintering (abbreviated as PECS) is a newly developed pressure-sintering process, which is used to consolidate ceramics, metals and their composites. This process is commercially named as plasma activated sintering (PAS) or spark plasma sintering (SPS). In the PECS process, a raw powder is placed inside an electrically conductive die, the unit is closed with two punches pressed uniaxially, and an electric current is momentarily applied through the electrically conductive die, in some cases, through the sample to heat the specimen [5–39]. The PECS process to fabricate transparent ceramics is being widely applied [26–36], especially in the sintering of transparent Al_2O_3 [29–36]. In particular, it was demonstrated that a low heating rate is efficient for densification and transparency in PECS of Al_2O_3 [34–36].

However, there has been no report on sintering of colored Al_2O_3 such as ruby by PECS. In the present study, an Al_2O_3–Cr_2O_3 powder mixture was prepared by drying an aqueous slurry consisting of Al_2O_3 and $Cr(NO_3)_3$. The effects of heating rate, applied pressure and sintering temperature were investigated on densification, grain growth and transparency of Cr-doped Al_2O_3 polycrystals prepared by PECS.

2. Experimental procedure

Commercially available α-Al_2O_3 powder (99.99% purity, TM-DAR, Taimei Chemicals Co. Ltd., Japan) and $Cr(NO_3)_3$ (Nacalai Tesque Inc., Japan) as a source material of Cr_2O_3, were used in the present study. For preparing the Al_2O_3–Cr_2O_3 powder mixture, an aqueous slurry consisting of α-Al_2O_3 powder and $Cr(NO_3)_3$ in distilled water was dried by dropping it into a glassware pot heated at 350 °C. The Cr_2O_3 concentration in the final powder mixture was fixed to be 70 ppm in mass fraction. The Al_2O_3–Cr_2O_3 powder mixture was ground by dry-milling with an alumina mortar for 30 min.

* Corresponding author. Tel.: +81 258 47 9709; fax: +81 258 47 9770.
E-mail address: nanko@mech.nagaokaut.ac.jp (M. Nanko).

0272-8842/$36.00
doi:10.1016/j.ceramint.2010.11.009

The sintering experiments were conducted by using Dr. Sinter Model SPS-1050 (Sumitomo Coal Mining Co.). The pulse pattern was set at 12/2 in ON/OFF time which means those 12 pulses of electric current (ON) go through the die/sample followed by 2 pulses of no electric current (OFF) with the same pulse duration of 3.3 ms for achieving minimum grain growth [37–39]. The starting powder was placed into a high-density graphite die (outer diameter of 30 mm, inner diameter of 15.4 mm and height of 30 mm) having a 1.8 mm in diameter and 3 mm depth hole in the outside surface for temperature monitoring. Graphite sheets of 0.1 mm thick were inserted between the die/punch and the powder. Die temperature (sintering temperature) was controlled by a preset heating program and it was measured by an optical pyrometer focused on the surface hole of the die during heating. The PECS was conducted at the die temperatures ranging from 1100 to 1300 °C for 20 min with various heating rates from 2 to 100 °C/min in vacuum. A uniaxial pressure was applied from 40 to 100 MPa. Similar to previous studies [6,8,37–39], the sample temperature was measured by a type-R thermocouple, which was inserted through a hole drilled in the punches. The sintered samples were polished carefully like mirror surface using finer diamond slurry grains (1 μm). The final thickness of all samples was approximately 2.5 mm.

Bulk density of as-sintered sample was measured by the liquid displacement technique with toluene. The relative density was calculated from the measured bulk density to the theoretical density. The microstructure of ruby polycrystals was observed on the fractured surface by scanning electron microscopy (SEM) after breaking the sintered sample. The grain size of sintered bodies was determined by measuring the average cross-section area per grain and spherical grain assumption in the SEM images of the fractured surface. The measured grain size was then multiplied by 1.126 to determine the average grain size [40].

3. Results and discussion

3.1. Effects of applied pressure and heating rate

The relationship between the relative density of sintered samples and the applied pressure is depicted in Fig. 1. The relative density increases with increasing applied pressure. The relative density of ruby polycrystals sintered with the slowest heating rate was higher than that in the rapid heating rate under the same applied pressure. By applying uniaxial pressure of 100 MPa, all the samples attained nearly complete densification (over 99%). With an applied pressure of 80 MPa and higher, fully densified samples would be already obtained at the slowest heating rate. Pressure and heating rate appear to play the predominant role in densification.

Fig. 2 presents SEM images of fractured surface of ruby polycrystals sintered under various conditions. With an applied pressure of 40 MPa, the microstructure of all sintered samples exhibit number of pores at grain boundary junction and small grain size. Increasing pressure to 100 MPa, the sample with a heating rate of 2 °C/min is completely densified. Less pores and finer grains formed after sintering under higher pressure and slow heating rate. The pressure/heating rate and average grain size relationship is shown in Fig. 3. Applied pressure appears to weakly affect the average grain size while the heating rate significantly affected the average grain size. The grain size of ruby polycrystals with slower heating rate was smaller than the ones formed by the rapid heating rate. The heating rate played a greater role in grain growth than the applied pressure did.

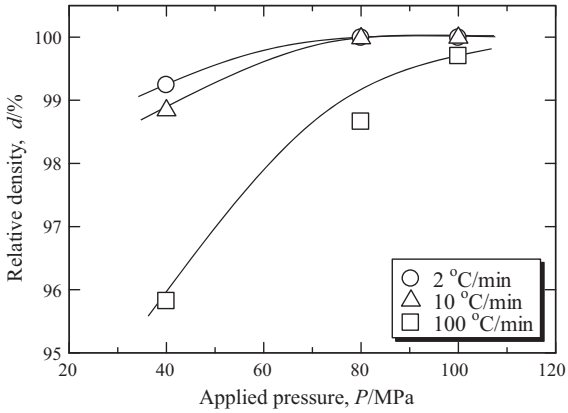

Fig. 1. Relationship between the relative density, d, and the applied pressure, P, for ruby polycrystals sintered at 1200 °C.

As presented in Fig. 3, the grain size with rapid heating rate was larger than those with a slower heating rate under the same applied pressure. This could be explained by a difference in temperature of the samples sintered in each heating rate. Fig. 4 shows the sample temperature as a function of the die temperature for PECS of powder mixture at the heating rates of 2 and 100 °C/min. PECS with a rapid heating rate had a higher sample temperature than that with a slow heating rate and it was also higher than the die temperature. The sample with a rapid heating rate has temperature about 50 °C higher than that of a slow heating rate at 1200 °C of die temperature. At this temperature, the difference of temperature in the samples using a slow heating rate was reached to approximately 60 °C higher in comparison to the die temperature. The difference in temperature between a sample and the die in various heating rates became larger as the die temperature increased. The result suggested that a high sample temperature results in a large grain size [37–39].

For the effect of the heating rate on the grain size, there have been conflicting results. Some researchers reported that the grain size of Al_2O_3 decreased as the heating rate increased [10,12,45]. Those reports mentioned a small grain size at rapid heating for Al_2O_3, which was opposite to the results of the present study and other studies [34,35,46]. The different types of Al_2O_3 powders and different sintering conditions may provide a clue for understanding the conflicting results. To explain the reason for larger grain size at the rapid heating rate, Murayama and Shin argued that a high defect concentration had been produced by rapid heating and associated rapid plastic deformation during densification [46] that was suggested to accelerate the grain growth during PECS processing.

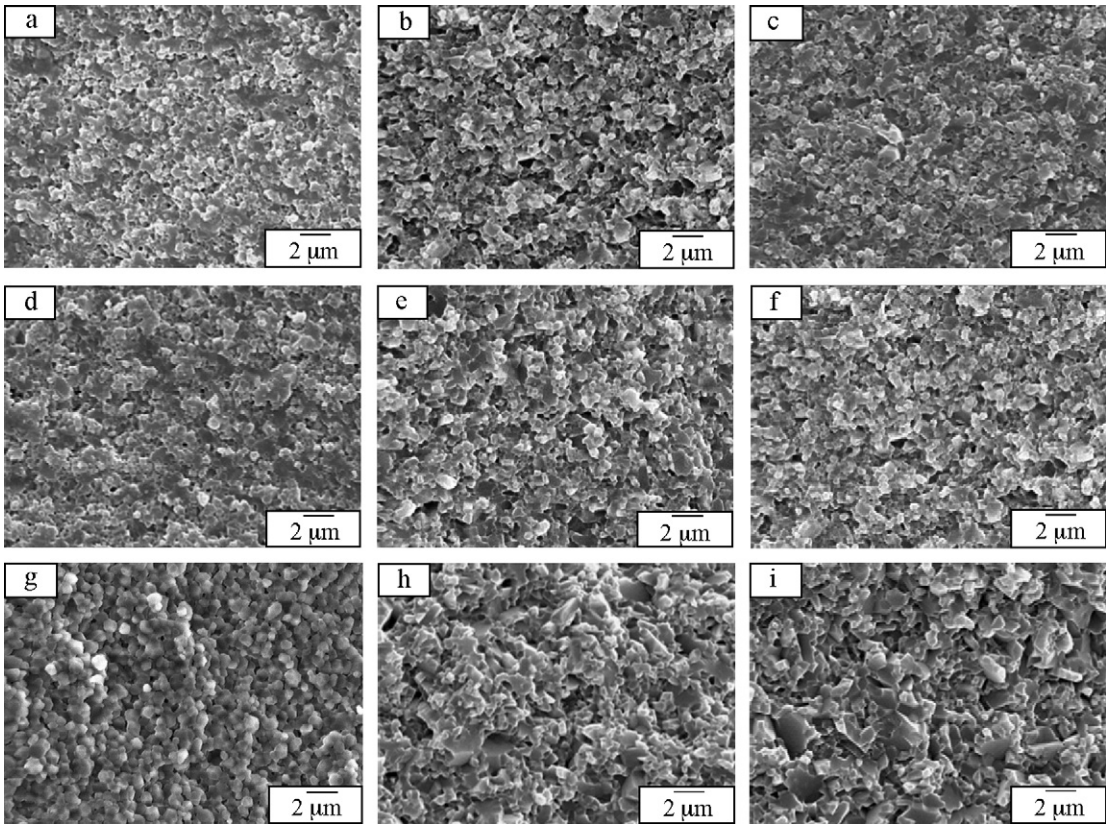

Fig. 2. Microstructures of the fractured surface of ruby polycrystals sintered at 1200 °C: (a)–(c) a heating rate of 2 °C/min and the applied pressures of 40, 80 and 100 MPa; (d)–(f) a heating rate of 10 °C/min and the applied pressures of 40, 80 and 100 MPa and (g)–(i) a heating rate of 100 °C/min and the applied pressures of 40, 80 and 100 MPa, respectively.

3.2. Effects of sintering temperature

While a difference in temperature between the sample and the die is often qualitatively acknowledged, the reported experimental results are based on both temperatures. Fig. 5 shows the relative density of sintered bodies as a function of the die temperature for ruby polycrystals sintered with various heating rate and under an applied pressure of 100 MPa. The relative density increased as the die temperature increased. At the same die temperature, the comparison indicated that PECS with a slow heating rate achieved a higher density than that with a rapid heating rate. As the result, the complete densification of ruby polycrystals was obtained when the die temperature was above 1200 °C for all heating rates. In the densification of ruby polycrystals, it was clear that PECS with a high die temperature and a slow heating rate offered a more significant densification than that with a low die temperature and a rapid heating rate.

SEM images of fractured surfaces of ruby polycrystals sintered with various heating rate at difference sintering

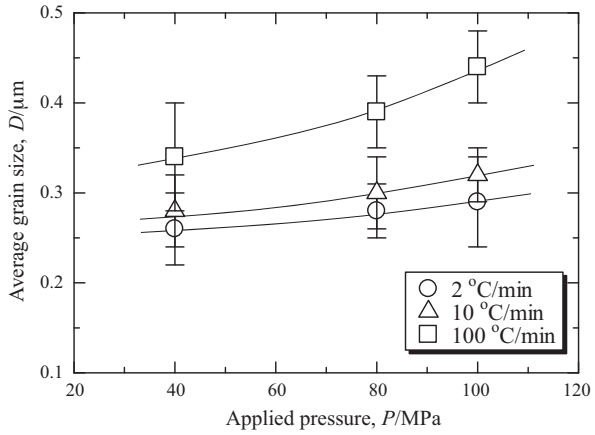

Fig. 3. Relationship between the average grain size, D, and the applied pressure, P, for ruby polycrystals sintered at 1200 °C. The error bars show maximum and minimum values.

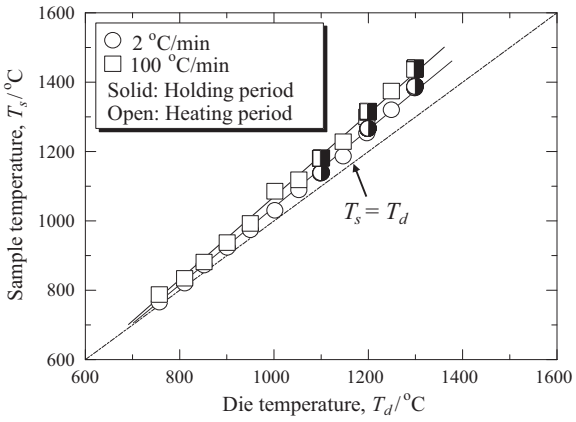

Fig. 4. Sample temperature, T_s, as a function of the die temperature, T_d, for ruby polycrystals sintered under an applied pressure of 100 MPa.

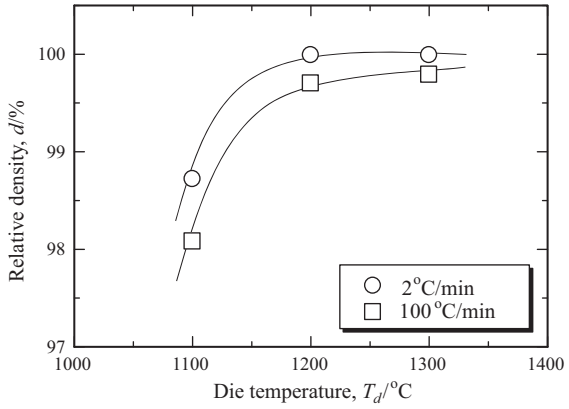

Fig. 5. Relationship between the relative density, d, and the die temperature, T_d, for ruby polycrystals sintered under an applied pressure of 100 MPa.

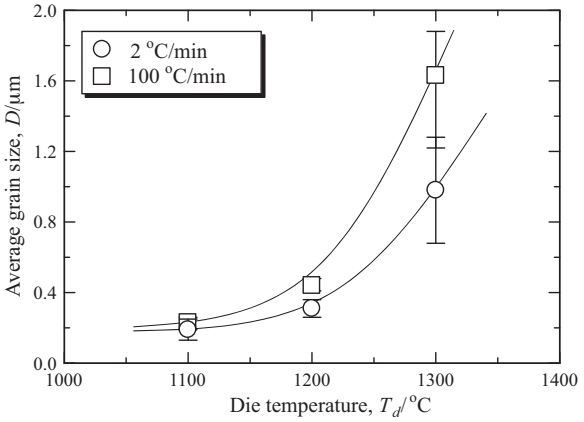

Fig. 7. Relationship between the average grain size, D, and the die temperature, T_d, of ruby polycrystals sintered under an applied pressure of 100 MPa. The error bars show maximum and minimum values.

temperature are presented in Fig. 6. In the case of a die temperature of 1100 °C, there exist a number of pores inside the samples with a low relative density for various heating rates (Fig. 6(a) and (d)). The average grain size of these samples was still as fine as the particle size of the Al_2O_3–Cr_2O_3 powder mixture. Larger grains were found in the ruby polycrystals sintered at a higher die temperature. At the die temperature of 1300 °C, rapid grain growth occurred (Fig. 6(c) and (f)). The average grain size increases with increasing die temperature for various heating rates is shown in Fig. 7. The results indicate that the average grain size of a rapid heating rate was larger than that of a slow heating rate at the same die temperature. This difference is clearly seen at a higher die temperature. For the ruby polycrystals sintered at 1300 °C, the average grain size was 4–5 times larger than that of the sample sintered at a lower sintering temperature. Thus, changes in the heating rate gave rise to differences in microstructures of ruby polycrystals sintered at the same die temperature. The larger grain size may indicate a higher temperature or higher grain boundary mobility inside the sample. The die temperature showed a major effect on densification and grain growth of ruby polycrystals sintered by PECS processing.

The dependence of the sample temperature on the relative density and the grain growth for various heating rates is shown in Fig. 8(a) and (b), respectively. An increase in the relative density with an increasing sample temperature can be observed. The increase in the density appeared to be minor when the sample temperature is higher than 1300 °C regardless of the heating rate. Besides, when the sample temperature increased, the relative density of ruby polycrystals sintered by a slow heating rate is higher than those achieved by a rapid heating rate, as shown in Fig. 8(a). The difference appeared to decrease as the sample temperature increased. Obviously, the experimental condition of a high sample temperature and a slow heating rate gave more advantages than a low sample temperature and a rapid heating rate in the densification of ruby polycrystals. Both the heating rate and the sample temperature had effects on densification. However, the grain growth was independent of the heating rate though the sample

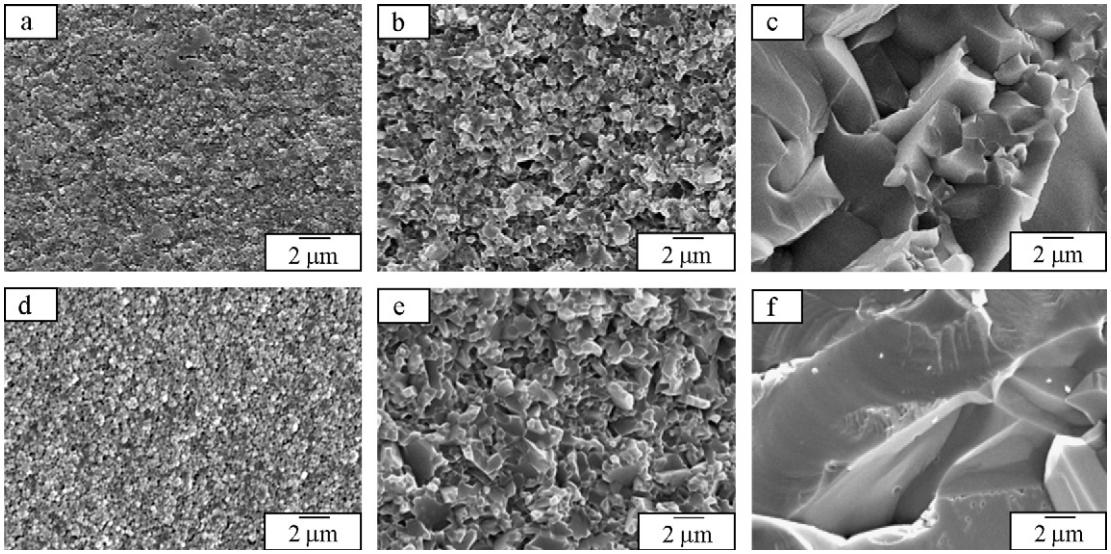

Fig. 6. Microstructures of the fractured surface of ruby polycrystals sintered under an applied pressure of 100 MPa: (a)–(c) a heating rate of 2 °C/min and the die temperatures of 1100 °C, 1200 °C and 1300 °C; (d)–(f) a heating rate of 100 °C/min and the die temperatures of 1100 °C, 1200 °C and 1300 °C, respectively.

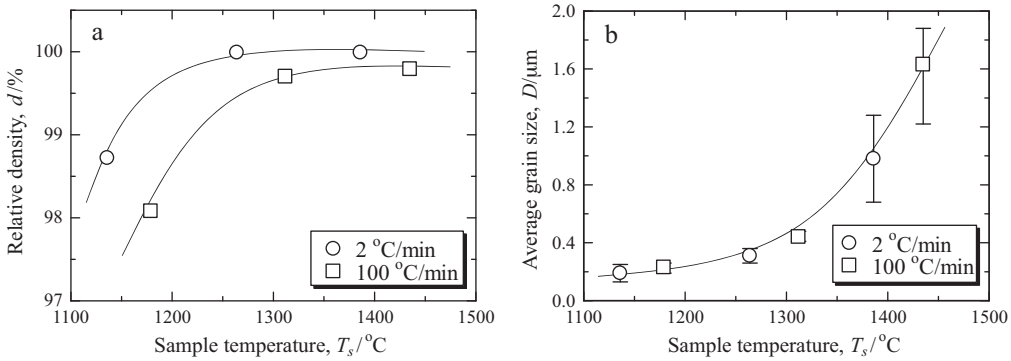

Fig. 8. Sample temperature, T_s, dependence of the (a) relative density, d; and (b) average grain size, D, of the ruby polycrystals sintered under an applied pressure of 100 MPa. The error bars show maximum and minimum values.

temperature was the same. As presented in Fig. 8(b), a further increase in the sample temperature resulted in a further increase in the average grain size even at different heating rates. The grain growth became significant when the sample temperature was above 1350 °C.

3.3. Transparency

Fig. 9 shows the sample images of ruby polycrystals sintered by PECS. As mentioned above, a higher applied pressure and a slower heating rate resulted in a complete densification and small grain size. The transparency of ruby polycrystals could be affected by both the relative density and the grain size. Since the transparency is inversely proportional to the grain size and is directly proportional to the density [29–32,41–44], the transparency of the ruby polycrystals was intensified when the pressure increased and the heating rate decreased. The ruby polycrystals with low density had lower apparent transparency than the dense ones. In addition, not only the effects of density but also the grain size influenced the transparency of ruby polycrystals. When increasing the pressure and simultaneously decreasing the heating rate, the appearance of ruby polycrystals changed gradually from opaque to highly transparent. The excellent transparency of ruby polycrystals was obtained at a sintering temperature of 1200 °C with a heating rate of 2 °C/min and under an applied

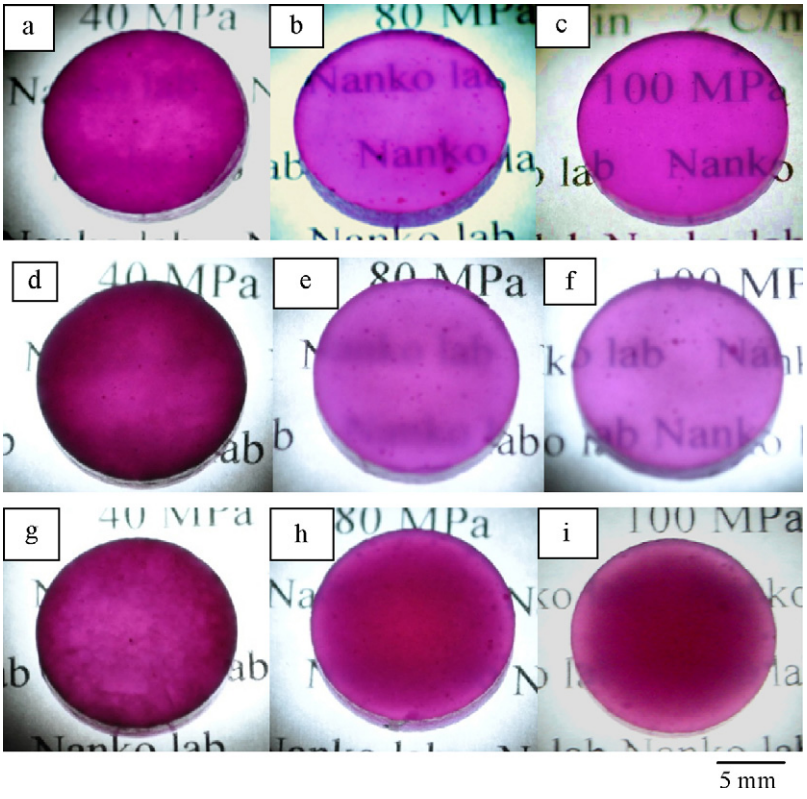

Fig. 9. Images of ruby polycrystals sintered at 1200 °C: (a)–(c) a heating rate of 2 °C/min and the applied pressures of 40, 80 and 100 MPa; (d)–(f) a heating rate of 10 °C/min and the applied pressures of 40, 80 and 100 MPa and (g)–(i) a heating rate of 100 °C/min and the applied pressures of 40, 80 and 100 MPa, respectively. All the samples are placed directly on the text.

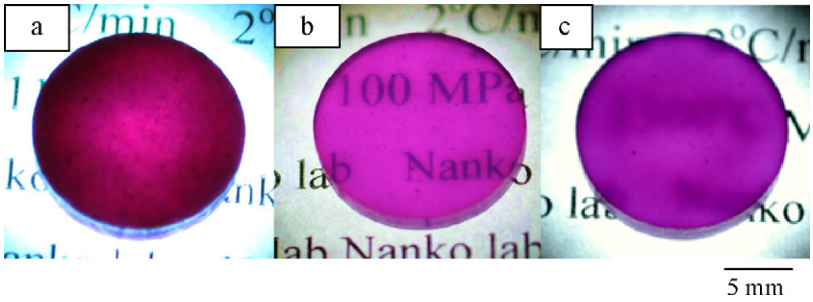

Fig. 10. Images of ruby polycrystals sintered with a heating rate of 2 °C/min and under an applied pressure of 100 MPa: (a) 1100 °C in sintering temperature, (b) 1200 °C and (c) 1300 °C. All the samples are placed directly on the text.

pressure of 100 MPa (Fig. 9(c)). The transparency of ruby polycrystals is easily evaluated by the naked eyes.

The appearance of ruby polycrystals sintered with a heating rate of 2 °C/min and under an applied pressure of 100 MPa at various sintering temperature is shown in Fig. 10. The ruby polycrystalline material sintered at 1200 °C (Fig. 10(b)) shows a clearer underlying image than the ones sintered at 1100 °C (Fig. 10(a)). This is due to an increase in the densification of the sample, as mentioned in the previous section. At a sintering temperature of 1300 °C (Fig. 10(c)), the ruby polycrystals changed from transparent to translucent. This phenomenon can be explained by pore growth caused by rapid grain growth occurred inside the sample [33,36,42].

4. Conclusions

PECS of transparent Cr-doped Al_2O_3 was investigated. Highly densified Cr-doped Al_2O_3 polycrystalline material was successfully obtained by using PECS processing. In this study, the applied pressure weakly influenced grain growth, but its effect on the densification has been significant. At the same die temperature, the heating rate affected sample temperature, densification and grain growth of the ruby polycrystals. However, at the same sample temperature, the grain growth was independent of the heating rate. The densification and the grain growth affected the transparency of the sintered sample. The sintered ruby polycrystals at a sintering temperature of 1200 °C with a slow heating rate, e.g. 2 °C/min and a high applied unixial pressure, e.g. 100 MPa, showed excellent transparency which was easily visible by the naked eyes. Owing to grain growth, the ruby polycrystals sintered at 1300 °C changed from transparent to translucent.

References

[1] A. Krell, T. Hutzler, J. Klimke, Transmission physics and consequences for materials selection, manufacturing, and applications, J. Eur. Ceram. Soc. 29 (2009) 207–221.
[2] E.R. Dobrovinskaya, L.A. Lytvynov, V. Pishchik, Sapphire: Material, Manufacturing, Applications, Springer, New York, 2009.
[3] C.E. Taylor, C.E. Bowman, W.P. North, W.F. Swinson, Applications of lasers to photoelasticity, Exp. Mech. 6 (1966) 289–296.
[4] J.R. Alcala, S.C. Liao, J. Zheng, Real time frequency domain fibreoptic temperature sensor using ruby crystals, Med. Eng. Phys. 18 (1996) 51–56.
[5] M. Tokita, Trends in advanced SPS spark plasma sintering systems and technology, J. Soc. Powder Technol. Jpn. 30 (1993) 790–804.
[6] M. Nanko, T. Maruyama, H. Tomino, Neck growth on initial stage of pulse current pressure sintering for coarse atomized powder made of cast-iron, J. Jpn. Inst. Metals 63 (1999) 917–923.
[7] M. Nanko, T. Oyaidu, T. Maruyama, Densification of Ni-20Cr alloy course-powder by pulse current pressure sintering, J. Jpn. Inst. Met. 66 (2002) 87–93.
[8] M. Sato, M. Nanko, K. Matsumaru, K. Ishizaki, Homogeneity in sintering of fine Ni-20Cr powder by pulsed electric current sintering (PECS) process, Adv. Tech. Mater. Mater. Proc. J. 8 (2006) 101–108.
[9] G.D. Zhan, J. Kuntz, J. Wan, J. Garay, A.K. Mukherjee, Alumina-based nanocomposites consolidated by spark plasma sintering, Scripta Mater. 47 (2002) 737–741.
[10] Z. Shen, M. Johnsson, Z. Zhao, M. Nygren, Spark plasma sintering of alumina, J. Am. Ceram. Soc. 85 (2002) 1921–1927.
[11] T. Kondo, T. Kuramoto, Y. Kodera, M. Ohyanagi, Z.A. Munir, Enhanced growth of Mo_2C formed in Mo–C diffusion couple by pulse DC current, J. Jpn. Soc. Powder Powder Metall. 55 (2008) 643–650.
[12] Y. Zhou, K. Hirao, Y. Yamauchi, S. Kanzaki, Densification and grain growth in pulse electric sintering of alumina, J. Eur. Ceram. Soc. 24 (2004) 3465–3470.
[13] S.W. Wang, L.D. Chen, T. Hirai, Densification of Al_2O_3 powder using spark plasma sintering, J. Mater. Res. 15 (2000) 982–987.
[14] D. Jiang, D.M. Hulbert, J.D. Kuntz, U. Anselmi-Tamburini, A.K. Mukherjee, Spark plasma sintering: a high strain rate low temperature forming tool for ceramics, Mater. Sci. Eng. A 463 (2007) 89–93.
[15] F. Guillard, A. Allemand, J. Lulewicz, J. Galy, Densification of SiC by SPS-effects of time, temperature and pressure, J. Eur. Ceram. Soc. 27 (2007) 2725–2728.
[16] M. Suganuma, Y. Kitagawa, Pulsed electric current sintering of silicon nitride, J. Am. Ceram. Soc. 86 (2003) 387–394.
[17] S.W. Wang, L.D. Chen, T. Hirai, J. Guo, Formation of Al_2O_3 grains with different sizes and morphologies during the pulse electric current sintering process, J. Mater. Res. 16 (2001) 3514–3517.
[18] D.M. Zhang, Z.Y. Fu, Y.C. Wang, Q.J. Zhang, J.K. Guo, Heterogeneous of non-conductive materials sintering by pulse electric current, Key Eng. Mater. 224–226 (2002) 729–734.
[19] D. Zhang, L. Zhang, Z. Fu, J. Guo, W.H. Tuan, Differential sintering of Al_2O_3/ZrO_2–Ni composite, during pulse electric current sintering, Ceram. Int. 32 (2006) 241–247.
[20] W. Zhou, B. Mei, J. Zhu, Fabrication of high-purity ternary carbide Ti_3AlC_2 by spark plasma sintering (SPS) technique, Ceram. Int. 33 (2007) 1399–1402.
[21] T. Isobe, K. Daimon, T. Sato, T. Matsubara, Y. Hikichi, T. Ota, Spark plasma sintering technique for reaction sintering of Al_2O_3/Ni nanocomposite and its mechanical properties, Ceram. Int. 34 (2008) 213–217.
[22] S. Guo, Y. Kagawa, T. Nishimura, H. Tanaka, Elastic properties of spark plasma sintered (SPSed) ZrB_2–ZrC–SiC composites, Ceram. Int. 34 (2008) 1811–1817.
[23] Y.L. Li, J. Zhang, J.X. Zhang, Fabrication and thermal conductivity of AlN/BN ceramics by spark plasma sintering, Ceram. Int. 35 (2009) 2219–2224.
[24] S. Hayun, S. Kalabukhov, V. Ezersky, M.P. Dariel, N. Frage, Microstructural characterization of spark plasma sintered boron carbide ceramics, Ceram. Int. 36 (2010) 451–457.

[25] Norhayati Ahmad, Hidekazu Sueyoshi, Properties of Si_3N_4–TiN composites fabricated by spark plasma sintering by using a mixture of Si_3N_4 and Ti powders, Ceram. Int. 36 (2010) 491–496.
[26] R. Chaim, M. Kalina, J.Z. Shen, Transparent yttrium garnet (YAG) ceramics by spark plasma sintering, J. Eur. Ceram. Soc. 27 (2007) 3331–3337.
[27] R. Chaim, M. Kalina, J.Z. Shen, Transparent YAG ceramics by surface softening of nanoparticles in spark plasma sintering, Mater. Sci. Eng. A 429 (2006) 74–78.
[28] K. Morita, B.N. Kim, K. Hiraga, H. Yoshida, Fabrication of transparent $MgAl_2O_4$ spinel polycrystal by spark plasma sintering, Scripta Mater. 58 (2008) 1114–1117.
[29] D. Jiang, D.M. Hulbert, U. Anselmi-Tamburini, T. Ng, D. Land, A.K. Mukherjee, Optically transparent polycrystalline Al_2O_3 produced by spark plasma sintering, J. Am. Ceram. Soc. 91 (2008) 151–154.
[30] Y. Aman, V. Garnier, E. Djurado, Influence of green state processes on the sintering behaviour and the subsequent optical properties of spark plasma sintered alumina, J. Eur. Ceram. Soc. 29 (2009) 3363–3370.
[31] M. Suárez, A. Fernández, J.L. Menéndez, R. Torrecillas, Grain growth control and transparency in spark plasma sintered self-doped alumina materials, Scripta Mater. 61 (2009) 931–934.
[32] M. Stuer, Z. Zhao, U. Aschauer, P. Bowen, Transparent polycrystalline alumina using spark plasma sintering: effect of Mg, Y and La doping, J. Eur. Ceram. Soc. 30 (2010) 1335–1343.
[33] R.S. Dobedoe, G.D. West, M.H. Lewis, Spark plasma sintering of ceramics, Bull. Eur. Ceram. Soc. 1 (2003) 19–24.
[34] B.N. Kim, K. Hiraga, K. Morita, H. Yoshida, Spark plasma sintering of transparent alumina, Scripta Mater. 57 (2007) 607–610.
[35] B.N. Kim, K. Hiraga, K. Morita, H. Yoshida, Effects of heating rate on microstructure and transparency of spark plasma sintered alumina, J. Eur. Ceram. Soc. 29 (2009) 323–327.
[36] B.N. Kim, K. Hiraga, K. Morita, H. Yoshida, T. Miyazaki, Y. Kagawa, Microstructure and optical properties of transparent alumina, Acta Mater. 57 (2009) 1319–1326.
[37] K.Q. Dang, M. Nanko, Effects of ON/OFF pulse pattern on sintering alumina by a pulsed electric current sintering process, J. Ceram. Proc. Res. 10 (2009) s32–s38.
[38] K.Q. Dang, M. Nanko, M. Kawahara, S. Takei, Densification of alumina powder by using PECS process with different pulse electric current waveforms, Mater. Sci. Forum 620–622 (2009) 101–104.
[39] K.Q. Dang, M. Kawahara, S. Takei, M. Nanko, Effects of pulsed current waveforms on sample temperature and sintering behavior in PECS of alumina, J. Jpn. Soc. Powder Powder Metall. 56 (2009) 780–787.
[40] I. Mendelson, Average grain size in polycrystalline ceramics, J. Am. Ceram. Soc. 52 (1969) 443–446.
[41] R. Apetz, M.P.B. Bruggen, Transparent alumina: a light-scattering model, J. Am. Ceram. Soc. 86 (2003) 480–486.
[42] Y.T. O, J. Koo, K.J. Hong, J.S. Park, D.C. Shin, Effect of grain size on transmittance and mechanical strength of sintered alumina, Mater. Sci. Eng. A 374 (2004) 191–195.
[43] C. Pecharromàn, G. Mata-Osoro, L. Antonio Dìaz, R. Torrecillas, J.S. Moya, On the transparency of nanostructured alumina: Rayleigh-Gans model for anisotropic spheres, Opt. Express 17 (2009) 6899–6912.
[44] A. Braun, G. Falk, R. Clasen, Transparent polycrystalline alumina ceramic with sub-micrometre microstructure by means of electrophoretic deposition, Materialwiss. Werkstofftech. 37 (2006) 293–297.
[45] L.A. Stanciu, V.Y. Kodash, J.R. Groza, Effects of heating rate on densification and grain growth during field-assisted sintering of α-Al_2O_3 and $MoSi_2$ powders, Metall. Mater. Trans. A 32 (2001) 2633–2638.
[46] N. Murayama, W. Shin, Effect of rapid heating on densification and grain growth in hot pressed alumina, J. Ceram. Soc. Jpn. 108 (2000) 799–802.